

# Consolidating rock-physics classics: A practical take on granular effective medium models

Fabien Allo<sup>1</sup>

<https://doi.org/10.1190/tle38050334.1>

## Abstract

Granular effective medium (GEM) models rely on the physics of a random packing of spheres. Although the relative simplicity of these models contrasts with the complex texture of most grain-based sedimentary rocks, their analytical form makes them easier to apply than numerical models designed to simulate more complex rock structures. Also, unlike empirical models, they do not rely on data acquired under specific physical conditions and can therefore be used to extrapolate beyond available observations. In addition to these practical considerations, the appeal of GEM models lies in their parameterization, which is suited for a quantitative description of the rock texture. As a result, they have significantly helped promote the use of rock physics in the context of seismic exploration for hydrocarbon resources by providing geoscientists with tools to infer rock composition and microstructure from sonic velocities. Over the years, several classic GEM models have emerged to address modeling needs for different rock types such as unconsolidated, cemented, and clay-rich sandstones. We describe how these rock-physics models, pivotal links between geology and seismic data, can be combined into extended models through the introduction of a few additional parameters (matrix stiffness index, cement cohesion coefficient, contact-cement fraction, and laminated clays fraction), each associated with a compositional or textural property of the rock. A variety of real data sets are used to illustrate how these parameters expand the realm of seismic rock-physics diagnostics by increasing the versatility of the extended models and facilitating the simulation of plausible geologic variations away from the wells.

## Introduction

Based on the physics of a random packing of identical spheres, granular effective medium (GEM) models are an obvious analog for sedimentary rocks made of an aggregate of rounded mineral grains. They are a standard option for modeling sandstones made of quartz and feldspar grains or limestones formed from ooids, spherical calcite, or aragonite grains. Their simplicity of use is such that they are often applied beyond their original scope and associated assumptions when no better alternatives are available.

Most GEM models are hybrid models that combine several geologic concepts implemented through a mix of rigorous theories and heuristic techniques. A compaction trend captures the evolution of the elastic properties of a packing of grains during burial. Various contact models developed by Brandt (1955), Digby (1981), Walton (1987), and Jenkins et al. (2005) relate the elastic properties of a random aggregate of identical spheres to the normal and tangential stiffness of their grain-to-grain contacts. All derive from the original theory developed by Hertz (1882) and Mindlin (1949) to model the elastic behavior of two identical spheres in contact. An optional cementation trend formalized by Dvorkin et al. (1991) describes

the stiffening effect of cement deposited at grain contacts. An additional sorting trend defines the effect of porosity reduction due to the introduction of solid material in the interstitial pore space. This sorting trend is usually modeled through elastic bounds such as the ones defined by Hashin and Shtrikman (1963). To obtain saturated rock properties, the effect of the fluid present in the pore space is added through a transformation model such as the standard fluid substitution relations introduced by Gassmann (1951).

From a practical standpoint, the way these concepts are combined as well as the set of model parameters that can be adjusted are as important as the underlying theories and models. Parameters directly linked to rock composition and microstructure make the calibration to field data more intuitive and the quality control of predictions more objective. A geologically oriented parameterization also simplifies the integration of textural data obtained from cores, which mitigates part of the uncertainty inherent to the calibration process. We present how, through the introduction of a few physically meaningful parameters (matrix stiffness index [MSI], cement cohesion coefficient [CCC], contact-cement fraction [CCF], and laminated clays fraction [LCF]), classic GEM models can be combined into extended models suitable for improved rock-physics diagnostics over a broader range of formations. Particular attention is paid to the impact these parameters have on the modeled elastic rock properties. Often limited to rock-physics experts, this knowledge is key to achieving successful calibrations to field data. The potential for rock-physics diagnosis based on the extended models is demonstrated using a variety of real data sets. All illustrations focus on compressional wave velocity ( $V_p$ ), but the extended models also provide shear wave velocity ( $V_s$ ), which in combination with  $V_p$  is key to an accurate interpretation of lithology, pore fluid, and pore pressure from seismic data.

## Unconsolidated sandstone models

Dvorkin and Nur (1996) introduce the friable-sand or soft sandstone model to describe porosity-velocity relationships of poorly consolidated formations from the North Sea. This model uses a modified Hashin-Shtrikman lower bound to interpolate the bulk and shear moduli of the dry rock frame between the pure mineral and critical porosity end members. These bounds are defined by the moduli of the mineral grains and the pressure-dependent moduli of the dry pack of grains as given by the Hertz-Mindlin theory, respectively. The stiff sandstone model described by Mavko et al. (1998) shares the same end members but uses a modified Hashin-Shtrikman upper bound to interpolate between them. Combining these two models into an extended unconsolidated sandstone model is achieved by using a weighted modified Hashin-Shtrikman bound. The weighted bound allows linear interpolation between the moduli derived from the upper bound ( $M_{\text{stiff}}$ ) and the lower bound ( $M_{\text{soft}}$ ):

<sup>1</sup>CGG, Calgary, Alberta, Canada. E-mail: fabien.allo@cgg.com.

$$M = MSI \times M_{stiff} + (1 - MSI) \times M_{soft} \quad (1)$$

Used as weight factor in the interpolation, the MSI, ranging from 0 to 1, directly controls the stiffness of the rock at a given porosity as illustrated in Figure 1. In the case of composite mineral grains, MSI is also used as a weight in the computation of the effective grain moduli. High MSI values are indicative of well-consolidated sandstones characterized by fast velocities. Low MSI values suggest more poorly consolidated sandstones, exhibiting comparatively slower velocities. MSI can be related to the average pore aspect ratio in inclusion-based effective medium models, as both are indicators of the average stiffness of the rock frame. In addition to MSI, the two most sensitive parameters inherited from the original contact models are the critical porosity ( $\phi_c$ ) and the coordination number (C). The critical porosity introduced by Nur et al. (1998) separates two distinct elastic domains. Below  $\phi_c$  (load-bearing domain), the mineral grains are in contact and form a matrix that supports the pressure exerted on the rock. Above  $\phi_c$  (suspension domain), the rock breaks down into its individual constituents. The bulk modulus of the resulting suspension follows the Reuss bound, which assumes that grains and fluid are subject to the same stress. In the load-bearing domain, the Reuss bound gives a lower limit for the elastic moduli whereas the modified Voigt bound, based on the assumption that grains and pore fluid have the same strain, represents an upper limit irrespective of the geometry of grains and pores. Typical critical porosities for sandstones vary between 36% and 40% with stiffer rock frames characterized by higher critical porosities. The coordination number is the average number of contacts that each grain has with surrounding grains. Random aggregates of identical spheres, which are a good analog for well-sorted sediments, have

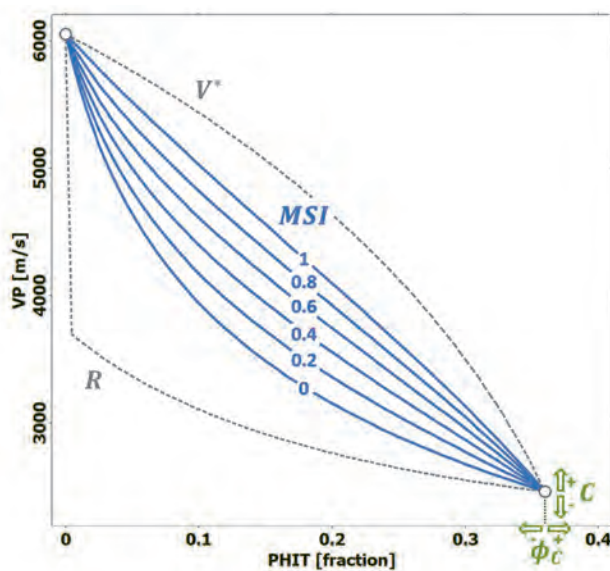
coordination numbers ranging from 7 (loose packing) to 9 (close packing) with higher coordination numbers translating into stiffer rock frames. Packs of spheres of various sizes, better suited to represent poorly sorted sediments, have higher coordination numbers, as small spheres occupy the pore space between larger spheres. Coordination numbers as high as 16 can be reached for packing with a broad grain-size distribution.

The Hertz-Mindlin theory relies on the hypotheses that all grains are spherical, of identical size, and that there is no slip between them. As most natural rocks violate these assumptions, Bachrach et al. (2000, 2008) extend the unconsolidated sandstone model to account for nonuniform contacts. While the practical impact of the effective contact radius parameter used to model grains of various sizes and shapes is usually limited, the ability to control friction between the grains through the fraction of nonslip contacts is of particular importance. As it only affects the shear modulus of the rock frame, this parameter proves useful to calibrate the dry rock  $V_p/V_s$  and Poisson's ratios, consistently underestimated by the original soft sandstone model that assumes a perfect adhesion between all grains.

Figure 2 illustrates how the extended unconsolidated sandstone model is able to reproduce observed velocity variations within the Ile Formation across three nearby fields in the North Sea, offshore Norway. Despite having similar mineralogy and porosity at a comparable depth, a clean brine-saturated sandstone interval exhibits distinct ranges of  $V_p$  across the fields, indicative of a variation of rock stiffness. Thin section photomicrographs reveal an evolution of rock texture from relatively large rounded grains to smaller angular grains, which correlates with the increase of rock stiffness interpreted from observed  $V_p$  and calibrated MSI.

### Cemented sandstone models

The contact-cement model introduced by Dvorkin et al. (1991) describes how cementation affects the elastic moduli of a random packing of spheres. This cementation trend captures stiffening of the rock frame as the amount of cement welding the grain increases. As a given rock sample contains a relatively constant amount of cement driven by its burial depth, Avseth (2000) and Avseth et al. (2000) combine this cementation trend with a sorting trend, modeled through a modified Hashin-Shtrikman lower bound, to produce the constant-cement model. The only parameter added to the contact-cement model is the volume of cement in the rock. The first few percent of cement cause a large velocity increase with little porosity reduction as shown in Figure 3. The spatial location of the cement, expressed through idealized deposition schemes, controls the rate of stiffening as more cement is deposited onto the grains. Table 1 summarizes the two original schemes introduced by Dvorkin et al. (1991) and introduces a new intermediate scheme, which depends on an additional parameter, the CCC, to interpolate between the two extreme cases. Theoretically, this coefficient, defined between 0 and 1, describes how effective the cement is at welding the grain contacts. In practice, it controls the derivative of the cementation trend at the critical porosity end member as illustrated in Figure 3. Chemical precipitation of quartz or calcite generally leads to stiff cementation schemes characterized by high CCC values, especially if the grains and cement share the same crystallographic structure. A mechanical deposition of



**Figure 1.** Rock-physics template (RPT) based on the extended unconsolidated sandstone model highlighting the impact of critical porosity ( $\phi_c$ ), coordination number (C), and MSI on  $V_p$  as a function of total porosity. The blue lines illustrate the impact of MSI and range from the soft sandstone line (MSI of 0) to the stiff sandstone line (MSI of 1). The green arrows indicate qualitatively how a modification of one of the other parameters would affect the template. The Reuss (R) and modified Voigt ( $V^*$ ) bounds (gray dotted lines) delimit the range of physically possible velocities based on the two given end members.

cement at the grain contacts, as is the case for clay coating, usually results in softer cementation schemes represented by lower CCC values. At equal porosity, mineralogy, and cement volume, rocks with higher CCC values exhibit faster seismic velocities.

In the case of slightly cemented rocks, not all grain contacts are cemented, which means that part of the matrix behaves as a cemented sandstone and the other part as an unconsolidated sandstone. Combining the two models into an extended cemented sandstone model is achieved by interpolating linearly between the moduli derived from the constant-cement model ( $M_{cem}$ ) and the unconsolidated sandstone model ( $M_{unc}$ ):

$$M = CCF \times (M_{cem} + \Delta_M) + (1 - CCF) \times M_{unc} \quad (2)$$

$$\Delta_M(\phi, \phi_C) = \frac{\phi}{\phi_C} (M_{unc}(\phi_C) - M_{cem}(\phi_C)) \quad (3)$$

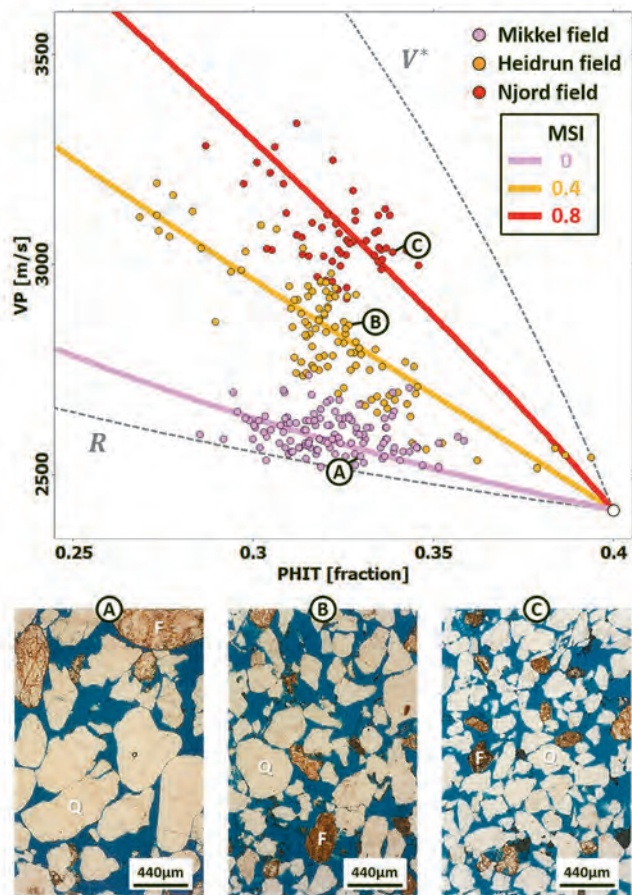
Used as weight factor in the interpolation, the CCF, ranging from 0 to 1, indicates the fraction of grain contacts actually welded

by cement. Combining these two models requires that both share the same end members. However, unlike the unconsolidated sandstone model, the constant-cement model is not pressure dependent. Equation 3 sets out the correction ( $\Delta_M$ ) applied to the constant-cement model in order to match the unconsolidated sandstone model prediction at the critical porosity end member where no cement has yet been introduced in the pore space. This correction is tapered linearly to take into account the fact that the moduli gradually become pressure independent as more cement is deposited in the pore space. Theoretically, a correction is also required at the pure mineral end member, but it can be omitted in practice as rocks with fully cemented pores have poor reservoir qualities and are therefore rarely of interest.

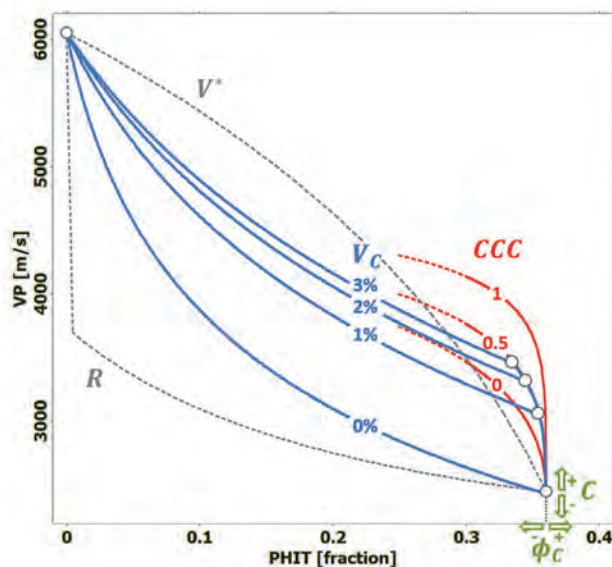
Figure 4 illustrates how the extended cemented sandstone model is able to reproduce the diagenetic trend observed in Njord Field, offshore Norway. Log data from three depth intervals follow distinct velocity-porosity trends consistent with increasing cement volume, CCC, and CCF, which suggests an intensification of cementation with depth. Thin sections, scanning electron microscope (SEM) images, and X-ray spectroscopy measurements support this diagnostic: as more quartz precipitates around the detrital grains, the cement distribution gradually evolves from an initial partial coating to a thicker layer that ultimately locks all grain contacts and occludes most of the effective porosity. This diagenetic trend is associated with a significant increase in velocity favorable for a detection based on seismic data.

### Clay-rich sandstone models

Most sandstones inherently include clay minerals due to their detrital origin. These minerals can have a substantial impact on the






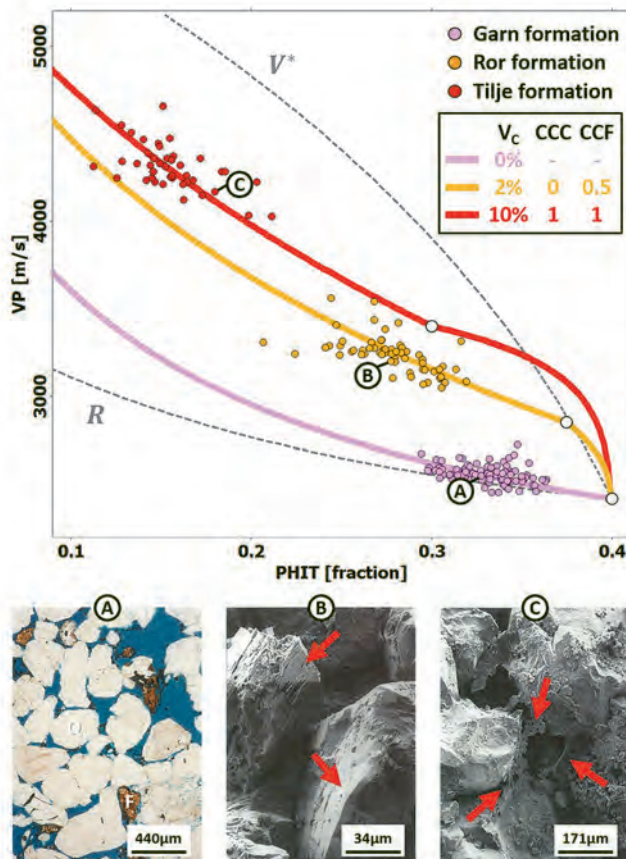
**Figure 2.**  $V_p$  variation observed in a clean brine-saturated sandstone interval within the Ile Formation across three nearby fields in the North Sea (top). Thin section photomicrographs (bottom) highlight an associated evolution of rock texture. The sandstone is composed of relatively large rounded grains of quartz (Q) and feldspar (F) at Mikkel (A) where recorded velocities are consistent with the soft sandstone model (pink line, MSI of 0). A mixture of large rounded and smaller angular grains at Heidrun (B) translates into faster velocities that fall around the orange line (MSI of 0.4). Small angular grains at Njord (C) correlate with even faster velocities that fall around the red line (MSI of 0.8).



**Figure 3.** RPT based on the extended cemented sandstone model highlighting the impact of critical porosity ( $\phi_c$ ), coordination number (C), volume of cement ( $V_c$ ), and CCC on  $V_p$  as a function of total porosity. The red lines represent various cementation trends ranging from the softest (CCC of 0) to the stiffest (CCC of 1) bound. The blue lines illustrate the impact of an increasing cement volume in the case of the intermediate cement deposition scheme (CCC of 0.5). Note how, at high porosities, predicted velocities can be higher than the modified Voigt ( $V^*$ ) bound, which represents an upper limit only for unconsolidated formations.

**Table 1.** The amount of contact-cement binding the grains ( $\alpha$ ) controls the stiffening of the rock frame. In the case of idealized cement deposition schemes, it can be expressed as a function of the coordination number ( $C$ ), the current porosity ( $\phi$ ), and the porosity when the cementation process started ( $\phi_0$ ). Dvorkin and Nur (1996) introduce two schemes that represent the stiffest (scheme 1) and softest (scheme 2) bounds for the cementation trend. The new intermediate scheme also depends on the CCC, which allows interpolating between the bounds (scheme 1 when CCC is equal to 1 and scheme 2 when CCC is equal to 0) to model more complex cement depositions observed in practice.

Cement deposition scheme	Amount of contact cement
Grain contact cement (scheme 1)	 $\alpha = 2 \left[ \frac{\phi_0 - \phi}{3C(1 - \phi_0)} \right]^{\frac{1}{4}}$
Intermediate scheme	 $\alpha = \left[ \frac{2(C + CCC(8 - C))(\phi_0 - \phi)}{3C(1 - \phi_0)} \right]^{\frac{2 - CCC}{4}}$
Coating cement (scheme 2)	 $\alpha = \left[ \frac{2(\phi_0 - \phi)}{3(1 - \phi_0)} \right]^{\frac{1}{2}}$



**Figure 4.** Diagenetic trend highlighted by three sandstone formations from the Njord Field. Data from the Garn Formation are consistent with the unconsolidated sandstone model (pink line), indicating a poorly consolidated formation. A thin section (A) confirms the absence of cement at this depth. Data from the Ror Formation, located 50 m deeper, fall close to the orange line, which suggests a slightly cemented sandstone. An SEM image (B) highlights the onset of thin quartz overgrowths (indicated by red arrows) on the detrital grains. Data from the Tilje Formation, located another 200 m deeper, exhibit much lower porosities and faster velocities and fall on average on the red line, indicative of a well-cemented sandstone. This is corroborated by an SEM image (C) in which all grain contacts are welded by thick quartz overgrowths (indicated by red arrows).

elastic properties of the sandstone when they occupy part of the pore space (dispersed clays) or form thin layers that disconnect the matrix grains (laminated clays). These effects are not taken into account in the previously discussed models, which only incorporate clays as part of the composite mineral grains (structural clays). Thomas and Stieber (1975) develop a model for the porosity of thinly bedded sands and shales by mixing clean high-porosity sand and low-porosity shale. Marion (1990) extends this concept to predict the seismic velocities of such an ideal binary mixture as a function of clay content. In addition to the volume of clays present in the rock frame, the position of the clay minerals in relation to the mineral grains is the most sensitive parameter of the model. Laminated clays organized in thin layers that disconnect the matrix grains are distinguished from dispersed clays that fill the interstitial pores between the grains

leaving the contacts intact. The elastic moduli of laminated clays follow a monotonic trend modeled by a Hashin-Shtrikman lower bound between the mineral and pure clay end members. Dispersed clays moduli exhibit a V-shaped behavior with the stiffest configuration reached at the apex of the V when the entire pore space is filled with clay particles. A Hashin-Shtrikman lower bound is also used to interpolate between the apex point and each of the two end members. A combination of these two idealized clay models proves useful to represent more intricate spatial organizations of clay minerals found in the field. It is achieved through a weighted harmonic average of the moduli derived from the laminated clays model ( $M_{lam}$ ) and the dispersed clays model ( $M_{disp}$ ):

$$M = \left[ \frac{LCF}{M_{lam}} + \frac{1 - LCF}{M_{disp}} \right]^{-1} \quad (4)$$

Used as weight factor in interpolation, the LCF, ranging from 0 to 1, indicates the fraction of clay minerals organized in thin layers in the rock. While our current implementation assumes the same mineral moduli for both dispersed and laminated clays, a straightforward extension would be to associate different clay minerals with the two textures (e.g., smectite for the laminated case versus illite or chlorite for the dispersed case) to reflect their distinct geologic origins. Figure 5 illustrates how the resulting clay-rich sandstone model is able to reproduce the distinctive V-shaped trends formed by log data sampling complete depositional cycles with varying fractions of laminated and dispersed clays. Figure 6 shows how this model was used to assess the probable spatial distribution of clay particles based on the velocity-porosity trend of log data from a deltaic depositional cycle located in the Great Australian Bight Basin, offshore Australia. This sequence of clean sandstone, shaly sandstone, silty shale, and pure shale is characterized by an increasing clay content caused by a gradual decrease in energy in the depositional environment. The pronounced V-shaped

trend exhibited by the log data suggests a predominance of dispersed clays in the shaly sandstone.

The presence of clay minerals can also have contrasting effects on the cementation of a rock during burial. In shallow sedimentary rocks, dispersed clays present in the pore space can act as soft cement, which reduces the potential slip between the mineral grains as a seismic wave propagates. In deeper sedimentary rocks, chemical precipitation of cement on the surface of the grains is often inhibited by a preexisting clay coating, which can lead to heterogeneous cementation depending on the position of the clay minerals relative to the framework grains. Similar complex cementation patterns can be caused by patchy oil saturation, as early hydrocarbon generation and diagenesis might occur simultaneously. Combining the clay-rich sandstone model and the cemented sandstone model in an extended clay-rich sandstone model is useful in these various cases. This is achieved by using the extended cemented sandstone model instead of the unconsolidated sandstone model to derive the mineral end member. Figure 7 illustrates how the original V-shaped template displayed in Figure 5 is modified when a few percent of cement is introduced.

Figure 8 shows how the extended clay-rich sandstone model was used to diagnose the spatial distribution of clay minerals and the degree of cementation throughout a transgressive deltaic depositional cycle in the Surat Basin, onshore Australia. A well-sorted medium-grained sandstone, located at the base of the sequence, exhibits higher than expected velocities given the compaction state, suggesting the presence of a significant amount of cement. Similar velocities but lower porosities in the shaly sandstones found in the lower Evergreen lead us to presume that dispersed clays occlude part of their porosity. Silty mudstones encountered in the upper Evergreen exhibit the same range of porosity as the shaly sandstones but slower velocities, indicating a larger proportion of laminated clays consistent with a deeper depositional environment. Core pictures of the various rock types encountered throughout the coarsening downward sequence support this qualitative rock-physics diagnostic.

### Limitations to the extent of rock-physics diagnostics

All the examples presented in this paper are favorable cases where reliable elastic properties (density and  $V_p$ ) and rock properties (porosity, mineralogy, and saturations) are available to calibrate the extended GEM models. Textural information obtained from cores, thin sections, and SEM images also helps constrain some of the model parameters. In such cases, calibration of the models is significantly simplified and rock-physics diagnostics based on them are more credible. Unfortunately, direct observation of the preserved rock structure is rarely possible, and wireline logs, often

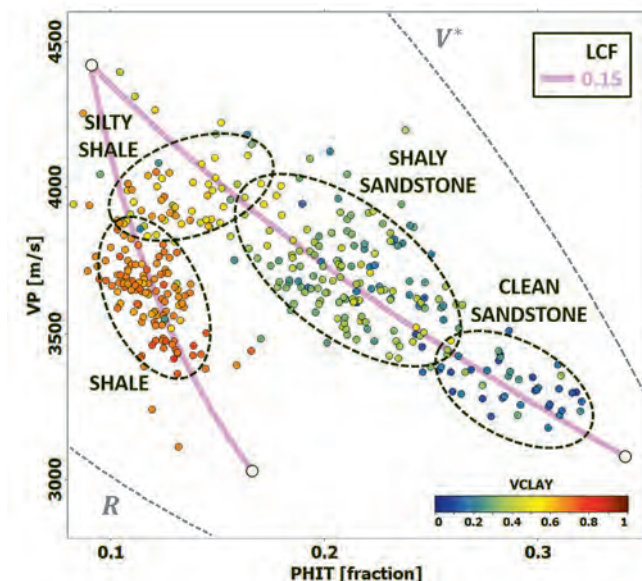


Figure 6. Log data from the Great Australian Bight Basin superimposed on an RPT based on the clay-rich sandstone model. The velocity-porosity trend, driven by an increasing amount of clays from the bottom to the top of the depositional cycle, follows on average the pink line defined by a fraction of laminated clays of 0.15. This suggests a predominance of dispersed clays in the intergranular porosity of the shaly sandstone (green points).

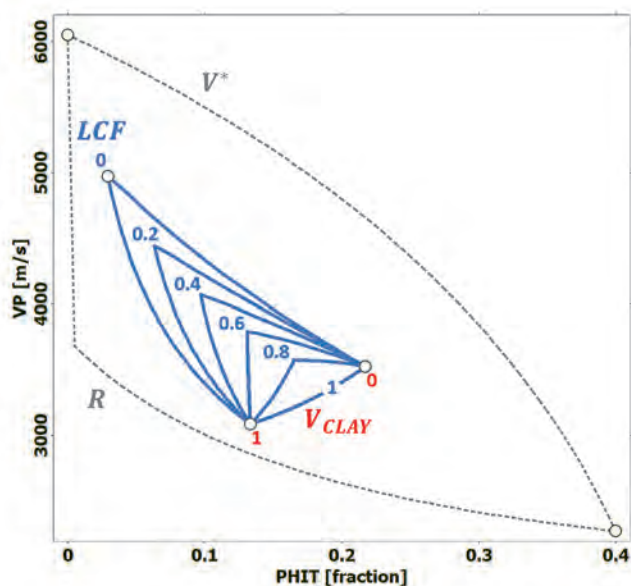


Figure 5. RPT based on the clay-rich sandstone model illustrating the impact of clay volume ( $V_{clay}$ ) and LCF on  $V_p$  as a function of total porosity.

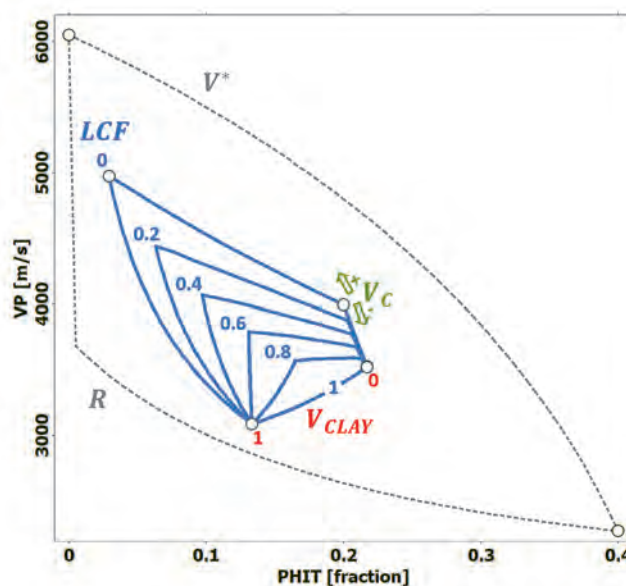


Figure 7. RPT based on the extended clay-rich sandstone model illustrating the impact of clay volume ( $V_{clay}$ ), LCF, and cement volume ( $V_c$ ) on  $V_p$  as a function of total porosity.

the sole source of information available, require careful processing before being used as calibration data. In practice, the predictive performance of all effective medium models is therefore limited by the quality of the input data available to calibrate them. The same is true of the accuracy of the rock-physics diagnostics based on them.

Other intrinsic limitations can affect the credibility of these diagnostics. A fundamental ambiguity exists when seeking a quantitative estimate of numerous unknown rock properties (such as porosity, pore geometry, mineralogy, saturations, etc.) from a limited number of independent elastic measurements (density and  $V_p$  in most cases). In that regard, the introduction of extra parameters in the extended GEM models increases uncertainty. Nevertheless, parameters that represent tangible rock properties allow for tighter quality control as unrealistic values, far from the expected range based on the available local geology information, are easier to detect. Data resolution is an additional source of uncertainty that prevents an accurate estimation of rock composition and microstructure, especially from seismic-derived elastic properties. Indeed, an infinity of combinations of different rock compositions and textures can lead to the same effective elastic properties at the seismic scale, rendering the inverse problem extremely nonunique. This usually

proves to be a tough challenge for deterministic petrophysical inversions, such as the one proposed by Bornard et al. (2005), which only provide a single estimate of rock properties that best match the recorded seismic data without quantification of the associated uncertainties. If statistical rock physics, through the simulation of a large number of possible scenarios, can help quantify these uncertainties, only the introduction of additional data (such as  $V_s$ , velocity attenuation, or directional velocities in the case of an anisotropic medium) can effectively lead to a more accurate estimation of the rock properties.

## Conclusions

Several classic GEM models used to represent unconsolidated, cemented, and clay-rich sandstones are combined into extended models applicable to a broader range of sedimentary formations. Built in these more versatile models, new parameters associated with compositional and textural properties of the rock, namely the matrix stiffness index, the cement cohesion coefficient, the contact-cement fraction, and the laminated clays fraction, enable a more detailed interpretation of the rock structure based on measured or seismic-derived elastic attributes. This geologically oriented parameterization also simplifies the integration of direct observations of the rock texture, which in turn reduces uncertainty associated with the calibration process. It also promotes an improved understanding between geologists and geophysicists and therefore helps mitigate some of the risks associated with any seismic exploration for hydrocarbon resources. ■■

## Acknowledgments

I thank CGG for the opportunity to write about this work and various colleagues for constructive suggestions that improved the paper. I am also grateful to CGG Multi-Client and New Ventures, Chevron, CTSCo, and the University of Queensland for providing the data used in the various figures.

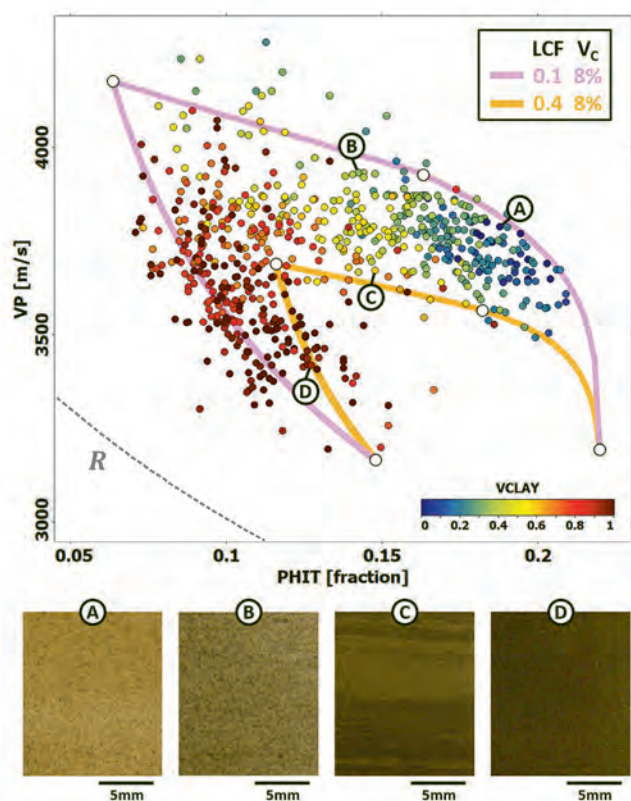
## Data and materials availability

Data used in Figures 2 and 4 are part of a North Sea multiclient study, which can be purchased (contact CGG Multi-Client and New Ventures). Data used in Figures 6 and 8 are proprietary client data. Access could be granted, pending client approval.

Corresponding author: fabien.allo@cgg.com

## References

- Avseth, P., 2000, Combining rock physics and sedimentology for seismic reservoir characterization in North Sea turbidite systems: PhD dissertation, Stanford University.
- Avseth, P., J. Dvorkin, G. Mavko, and J. Rykkje, 2000, Rock physics diagnostic of North Sea sands: Link between microstructure and seismic properties: *Geophysical Research Letters*, **27**, no. 17, 2671–2764, <https://doi.org/10.1029/1999GL008468>.
- Bachrach, R., J. Dvorkin, and A. M. Nur, 2000, Seismic velocities and Poisson's ratio of shallow unconsolidated sands: *Geophysics*, **65**, no. 2, 559–564, <https://doi.org/10.1190/1.1444751>.
- Bachrach, R., and P. Avseth, 2008, Rock physics modeling of unconsolidated sands: Accounting for nonuniform contacts and heterogeneous stress fields in the effective media approximation with



**Figure 8.** Log data from the Evergreen Formation in the Surat Basin superimposed on an RPT based on the extended clay-rich sandstone model. Most of the data fall between the pink and orange lines, suggesting a depositional cycle that includes a well-cemented sandstone, a shaly sandstone with a majority of dispersed clays, and a mudstone with a significant amount of laminated clays. Core pictures from Dawson et al. (2014) support this rock-physics diagnostic. A well-sorted cemented sandstone (A) forms the base of the sequence. Dispersed clays occlude part of the pore space of fine-grained sandstones (B) in the lower Evergreen, while thin beds of laminated clays are visible in silty mudstones (C) in the upper Evergreen. The sequence ends with a black organic-rich laminated mudstone (D).

- applications to hydrocarbon exploration: *Geophysics*, **73**, no. 6, E197–E209, <https://doi.org/10.1190/1.2985821>.
- Bornard, R., F. Allo, T. Coléou, Y. Freudenreich, D. H. Caldwell, and J. G. Hamman, 2005, Petrophysical seismic inversion to determine more accurate and precise reservoir properties: Presented at 14<sup>th</sup> Europec Biennial Conference, <https://doi.org/10.2118/94144-MS>.
- Brandt, H., 1955, A study of the speed of sound in porous granular media: *Journal of Applied Mechanics*, **22**, 479–486.
- Dawson, G. K. W., D. Biddle, S. M. Farquhar, J. Gao, S. D. Golding, X. Jiang, R. Keck, et al., 2014, Geochemical and geomechanical testing of near wellbore CO<sub>2</sub> injectivity improvement: Final Report, ANLEC Project 7-1110-0101, University of Queensland School of Earth Sciences.
- Digby, P. J., 1981, The effective elastic moduli of porous granular rocks: *Journal of Applied Mechanics*, **48**, no. 4, 803–808, <https://doi.org/10.1115/1.3157738>.
- Dvorkin, J., G. Mavko, and A. Nur, 1991, The effect of cementation on the elastic properties of granular material: *Mechanics of Materials*, **12**, no. 3–4, 207–217, [https://doi.org/10.1016/0167-6636\(91\)90018-U](https://doi.org/10.1016/0167-6636(91)90018-U).
- Dvorkin, J., and A. Nur, 1996, Elasticity of high-porosity sandstones: Theory for two North Sea data sets: *Geophysics*, **61**, no. 5, 1363–1370, <https://doi.org/10.1190/1.1444059>.
- Gassmann, F., 1951, Über die elastizität poröser medien: *Vierteljahrsschrift der Naturforschenden Gesellschaft in Zürich*, **96**, 1–23.
- Hashin, Z., and S. Shtrikman, 1963, A variational approach to the theory of the elastic behavior of multiphase materials: *Journal of the Mechanics and Physics of Solids*, **11**, no. 2, 127–140, [https://doi.org/10.1016/0022-5096\(63\)90060-7](https://doi.org/10.1016/0022-5096(63)90060-7).
- Hertz, H., 1882, Über die berührung fester elastischer körper: *Journal für die reine und angewandte Mathematik*, **92**, no. 1, 156–171.
- Jenkins, J., D. Johnson, L. La Ragione, and H. Makse, 2005, Fluctuations and the effective moduli of an isotropic, random aggregate of identical, frictionless spheres: *Journal of the Mechanics and Physics of Solids*, **53**, no. 1, 197–225, <https://doi.org/10.1016/j.jmps.2004.06.002>.
- Marion, D., 1990, Acoustical, mechanical, and transport properties of sediments and granular materials: PhD dissertation, Stanford University.
- Mavko, G., T. Mukerji, and J. Dvorkin, 1998, *The rock physics handbook*: Cambridge University Press.
- Mindlin, R. D., 1949, Compliance of elastic bodies in contact: *Journal of Applied Mechanics*, **16**, 259–268.
- Nur, A., G. Mavko, J. Dvorkin, and D. Galmudi, 1998, Critical porosity: A key to relating physical properties to porosity in rocks: *The Leading Edge*, **17**, no. 3, 357–362, <https://doi.org/10.1190/1.1437977>.
- Thomas, E. C., and S. J. Stieber, 1975, The distribution of shale in sandstone and its effect upon porosity: Presented at 16<sup>th</sup> Annual Logging Symposium, SPWLA.
- Walton, K., 1987, The effective elastic moduli of a random packing of spheres: *Journal of the Mechanics and Physics of Solids*, **35**, no. 2, 213–226, [https://doi.org/10.1016/0022-5096\(87\)90036-6](https://doi.org/10.1016/0022-5096(87)90036-6).